Search for the Decay $K^+ \to \pi^+ \gamma\gamma$

M. S. Atiya, I-H. Chiang, J. S. Frank, J. S. Haggerty, M. M. Ito,[a] T. F. Kycia, K. K. Li, L. S. Littenberg, A. J. Stevens, and R. C. Strand
Brookhaven National Laboratory, Upton, New York 11973

W. C. Louis
Medium Energy Physics Division, Los Alamos National Laboratory, Los Alamos, New Mexico 87545

D. S. Akerib, D. R. Marlow, P. D. Meyers, M. A. Selen,[b] F. C. Shoemaker, and A. J. S. Smith
Joseph Henry Laboratories, Princeton University, Princeton, New Jersey 08544

G. Azuelos,[c] E. W. Blackmore, D. A. Bryman, L. Felawka, P. Kitching, Y. Kuno, J. A. Macdonald, T. Numao, P. Padley, J-M. Poutissou, R. Poutissou, and J. Roy
TRIUMF, Vancouver, British Columbia, Canada V6T 2A3
(Received 30 May 1990)

A search for decays of the form $K^+ \to \pi^+ \gamma\gamma$ was performed for pion kinetic energies between 117 and 127 MeV. A 90%-C.L. upper limit for the branching ratio of $B(K^+ \to \pi^+ \gamma\gamma) < 1.0 \times 10^{-6}$ is set for direct decays assuming a π^+ energy distribution given by phase space. Limits are set for decays of the type $K^+ \to \pi^+ X^0$, $X^0 \to \gamma\gamma$, where X^0 is any short-lived neutral particle with mass smaller than 100 MeV/c^2.

PACS numbers: 13.40.Hq, 13.25.+m, 14.80.Gt

In this Letter we report the results of a search for the rare decay $K^+ \to \pi^+ \gamma\gamma$ from Experiment 787 at Brookhaven National Laboratory (BNL). This signature arises from the direct decay process $K^+ \to \pi^+ \gamma\gamma$ as well as from decays of the form $K^+ \to \pi^+ X^0$, $X^0 \to \gamma\gamma$, where X^0 is a massive short-lived neutral scalar particle.

Various approaches[1-4] have been proposed to describe the direct $K^+ \to \pi^+ \gamma\gamma$ decay. The predicted π^+ energy spectrum is model dependent and, in general, deviates significantly from that of pure phase space. Standard-model calculations performed in the framework of chiral perturbation theory[4] (ChPT) predict branching ratios in the range of 10^{-7}-10^{-6}.[5,6] The previous upper limit of $B(K^+ \to \pi^+ \gamma\gamma) < 8.4 \times 10^{-6}$ was determined from the kinematic region $117 \le T_{\pi^+} \le 127$ MeV, by assuming a pion phase-space spectrum.[7]

The possibilities for X^0 include a number of exotic particles postulated by various authors.[8] In addition, a light Higgs boson decaying via $H^0 \to \gamma\gamma$ could appear in this channel. The region of sensitivity for the X^0 mass m_{X^0} in this experiment is $0 < m_{X^0} < 100$ MeV/c^2. The previous upper limit for decays of this type is $B(K^+ \to \pi^+ X^0, X^0 \to \gamma\gamma) < 1.4 \times 10^{-6}$ for X^0 lifetimes shorter than 10^{-9} sec over a similar mass region.[7]

Using stopped positive kaons, we searched for a signal of the type $K^+ \to \pi^+ \gamma\gamma$ in the kinematic region $117 \le T_{\pi^+} \le 127$ MeV above the peak from $K^+ \to \pi^+ \pi^0$ decay ($T_{\pi^+} = 108.7$ MeV). This region was chosen to avoid backgrounds from $K^+ \to \pi^+ \pi^0$ decay that arise when the pion kinetic energy is reduced due to nuclear interactions in the stopping target. Potential sources of background are $K^+ \to \mu^+ \pi^0 \nu$, $K^+ \to \mu^+ \nu\gamma$ with an accidental photon, and the high-energy tail from $K^+ \to \pi^+ \pi^0$ that is due to detector resolution effects. $K^+ \to \mu^+ \pi^0 \nu$ and $K^+ \to \mu^+ \nu\gamma$ events were rejected by unambiguous identification of the charged pion and by kinematic constraints placed on the pion and the two photons. $K^+ \to \pi^+ \pi^0$ decays were removed by constraining kinematic variables such as the pion range, energy, and momentum.

The experiment used kaons from the low-energy separated beam line (LESB I) at the Alternating Gradient Synchrotron (AGS) at BNL. The cylindrically symmetric detector, whose side and end views are shown in Fig. 1, was designed primarily to search for the decay $K^+ \to \pi^+ \nu\bar{\nu}$ and is described elsewhere.[9] Briefly, a 775-MeV/c kaon beam was slowed by a BeO degrader and stopped in a segmented scintillating fiber target[10] located at the center of the detector. Charged decay products were momentum analyzed in a cylindrical central drift chamber[11] placed in a 1-T solenoidal magnetic field aligned along the detector axis. Once through the drift chamber they were stopped in a 15-layer scintillator range stack which surrounded the drift chamber. The 2-m-long plastic scintillators were viewed by phototubes at each end. These counters were used to measure the kinetic energy and range. Two layers of multiwire proportional wire chambers (RSPC) were imbedded in the range stack to provide additional measurements of the trajectories of charged tracks. Photons were detected in an electromagnetic calorimeter array consisting of a barrel section surrounding the range stack and a pair of end-cap sections located upstream and downstream of the drift chamber. The calorimeters consisted of alter-

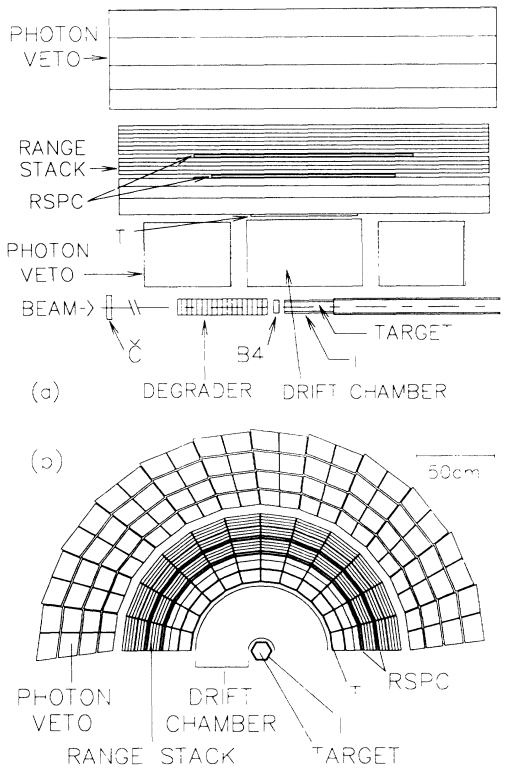

FIG. 1. (a) Side and (b) end views of the E787 detector.

nating layers of 1 mm lead and 5 mm scintillator and covered a solid angle of almost 4π. The barrel and end-cap arrays had total thickness of 14 and 12 radiation lengths, respectively. The barrel calorimeter had 48-fold azimuthal and 4-fold radial segmentation and the end cap had 24-fold azimuthal segmentation. The energy resolution of the calorimeters was $\sigma_E/E = 8/\sqrt{E}\,\%$ (E in GeV).

Range-stack scintillators in the pion stopping region were instrumented with transient digitizers[12] (TD's), which recorded phototube outputs every 2 nsec with an 8-bit dynamic range. The TD's covered a time window of ± 5 μsec with respect to the K^+ decay time, providing a complete history of the $\pi^+ \to \mu^+ \to e^+$ decay chain.

The trigger logic was organized in three levels of increasing complexity and decision time. The level-0 logic required a charged track to penetrate at least as far as the ninth layer of the range stack, but no further than the twelfth layer. This effectively imposed a range cut and eliminated most $K^+ \to \mu^+ \nu$ and $K^+ \to \pi^+ \pi^0$ events. Level 0 also demanded at least 5 MeV of visible photon energy in the barrel calorimeter or 10 MeV in the end-cap calorimeter. Finally, in-flight kaon decays were eliminated by requiring a decay time at least 2 nsec later than the kaon stopping time. The level-1 logic refined the range estimate of level 0 by taking into account the track angle, determined using the RSPC z information, and the target path length, determined by counting the number of struck target elements. Level 1 also required any additional range-stack energy outside the track to be less than 12 MeV. This "extra energy cut" eliminated events with photons showering in the range stack, thereby simplifying subsequent stages in the trigger and in the off-line analysis. The level-2 system included a microprocessor that summed the track energy in the range stack and in the target, rejecting events with track energy greater than 142 MeV. Level 2 also used the TD data from the pion stopping counter to distinguish pions from muons by looking for evidence of a second pulse arising from $\pi^+ \to \mu^+ \nu$ decay using a relationship between pulse height and pulse area.

The off-line analysis searched for a charged pion and two photon clusters consistent with the kinematics of $K^+ \to \pi^+ \gamma\gamma$. The program required exactly one positive charged track in the target, in the drift chamber, and in the range stack together with spatial matching at boundaries. To identify a pion, consistency of momentum, energy, and range with empirically determined expectations for pions was required. In addition, the TD information was used to observe the decay sequence of $\pi^+ \to \mu^+ \to e^+$ for definite pion identification, as described in Ref. 9. Further, in order to eliminate obvious $K^+ \to \pi^+ \pi^0$ events, minimum range and energy cuts were placed on the charged tracks.

The off-line time window for photons was ± 8 and ± 10 nsec with respect to the K^+ decay time for the barrel and end-cap calorimeters, respectively. Adjacent struck modules were grouped into a single cluster as one photon shower. The hit position in the plane perpendicular to the detector axis was determined by the azimuthal and radial segmentation of the calorimeter modules. The hit position along the detector axis in the barrel was calculated from end-to-end time and energy differences. The location of the photon shower was then obtained by an energy-weighted average of the hit positions of all modules belonging to the shower. Events that had fewer than two photon clusters with energy more than 1 MeV were rejected.

Remaining events were subjected to a kinematic fit for consistency with $K^+ \to \pi^+ \gamma\gamma$, including momentum and energy conservation. For the charged tracks, additional constraints required that the measured energy, range, and momentum were consistent with a pion hypothesis. Events that had a χ^2 confidence level $[P(\chi^2)]$ greater than 0.05 were accepted. The fit constraints served to eliminate $K^+ \to \mu^+ \pi^0 \nu$ and $K^+ \to \mu^+ \nu\gamma$ events, since the neutrino in such decays resulted in large missing energy. The invariant mass of the photon pair ($m_{\gamma\gamma}$) was calculated using the fitted values. The mass resolution thus obtained was evaluated with photons from π^0 decay in a clean $K^+ \to \pi^+ \pi^0$ sample, yielding a $\sigma_{m_{\gamma\gamma}} = 8$ MeV/c^2.

Figure 2 shows a plot of $m_{\gamma\gamma}$ vs $1 - P(\chi^2)$ for the final sample of events. The vertical band at the π^0 mass is due to $K^+ \to \pi^+ \pi^0$ events that leaked through the range

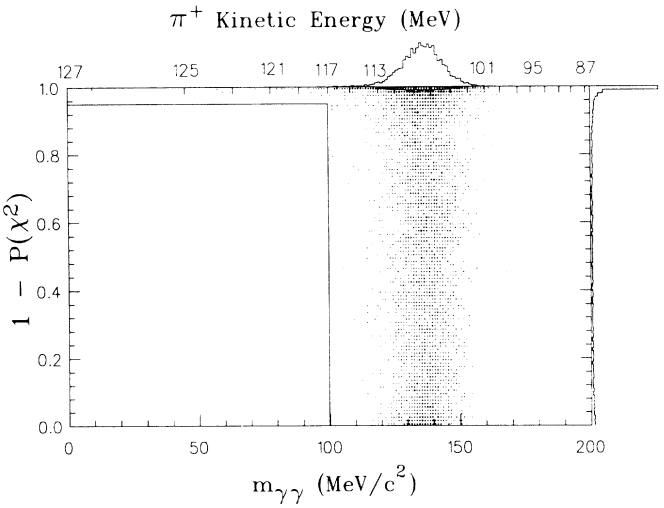

FIG. 2. Scatter plot of $m_{\gamma\gamma}$ vs $1-P(\chi^2)$ for the final sample of $K^+ \to \pi^+\gamma\gamma$ type of events.

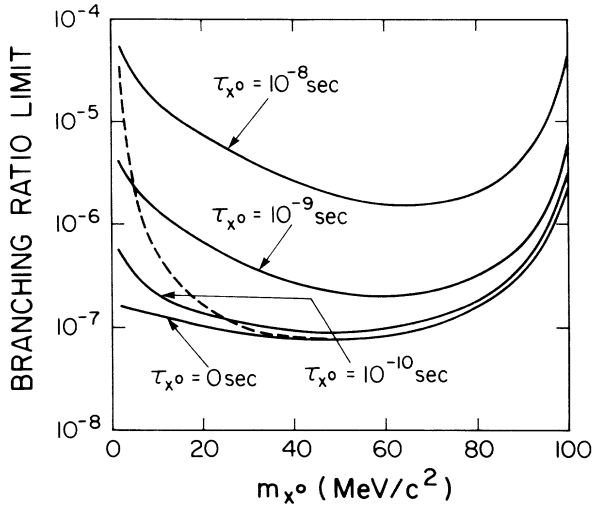

FIG. 3. The 90%-confidence-level upper limits for the branching ratio of $K^+ \to \pi^+X^0$, $X^0 \to \gamma\gamma$ for different X^0 lifetimes (τ_{X^0}) as a function of mass (m_{X^0}). The dashed curve shows the upper limit for the combined branching ratio for the Higgs-boson decay $K^+ \to \pi^+H^0$, $H^0 \to \gamma\gamma$.

and energy cuts of the trigger and the off-line analysis. The events concentrated at low $P(\chi^2)$ near the π^0 mass are either $K^+ \to \mu^+\pi^0\nu$ events or $K^+ \to \pi^+\pi^0$ events that suffered from pion scattering in the detector material or from leaking photons. A final kinematic cut was used to select a region of $0 \le m_{\gamma\gamma} \le 100$ MeV/c^2 and $1-P(\chi^2) \le 0.95$. There are no events found in this region as shown in Fig. 2, which corresponds to pion kinetic energies from 117 to the end point 127 MeV.

The data of Fig. 2 can be used to set limits on $K^+ \to \pi^+X^0$, $X^0 \to \gamma\gamma$. The acceptance was studied using Monte Carlo simulation and calibration data sets taken during the run. For example, the acceptance factors of the extra energy cut and of the kinematic fit were evaluated by using the data set of $K^+ \to \pi^+\pi^0$ decay. Table I shows the acceptance factors for $K^+ \to \pi^+X^0$, $X^0 \to \gamma\gamma$, in the case of a m_{X^0} of 50 MeV/c^2 and a X^0 lifetime (τ_{X^0}) of 10^{-10} sec. A total of 4.5×10^9 stopped kaons was accumulated for the present analysis. The overall systematic uncertainty in the acceptance is estimated to be $\pm 20\%$. We have checked our methods of calculating the acceptance by measuring the branching ratios for $K^+ \to \mu^+\nu$ and $K^+ \to \pi^+\pi^0$ and find consistency with established values.[9]

TABLE I. Acceptance factors for $K^+ \to \pi^+X^0$, $X^0 \to \gamma\gamma$ and $K^+ \to \pi^+\gamma\gamma$.

Category	π^+X^{0a}	$\pi^+\gamma\gamma$
Solid angle	0.21 ± 0.01	0.21 ± 0.01
π^+ spectrum	0.88 ± 0.09	0.074 ± 0.008
π^+ nuclear absorption	0.55 ± 0.02	0.55 ± 0.02
π^+ decay in-flight	0.92 ± 0.02	0.92 ± 0.02
$K^+ \to \pi^+$ delayed coincidence	0.79 ± 0.02	0.79 ± 0.02
$\pi^+ \to \mu^+$ TD tagging	0.61 ± 0.05	0.61 ± 0.05
$\mu^+ \to e^+$ TD tagging	0.79 ± 0.02	0.79 ± 0.02
Trigger efficiency	0.94 ± 0.04	0.94 ± 0.04
Extra energy cut	0.45 ± 0.01	0.45 ± 0.01
π^+ reconstruction	0.60 ± 0.04	0.60 ± 0.04
γ clustering and kinematic fit	0.61 ± 0.02	0.69 ± 0.02
Net acceptance	$(5.5 \pm 1.0)\times10^{-3}$	$(5.2 \pm 0.9)\times10^{-4}$

[a]The case of $m_{X^0} = 50$ MeV/c^2 and $\tau_{X^0} = 10^{-10}$ sec is shown.

Upper limits for X^0 for different lifetimes as a function of m_{X^0} are shown in Fig. 3. For instance, for X^0 with m_{X^0} of 50 MeV/c^2 and τ_{X^0} of 10^{-10} sec, the limit of 10^{-7} is almost a tenfold improvement over previous results. The limits for long-lived X^0 are higher because our acceptance falls off as the vertex of the $X^0 \to \gamma\gamma$ decay is displaced from the K^+ decay vertex. For smaller X^0 masses, the sensitivity drops due to merging of the two photons from the energy-boosted X^0. It is noted that a search for X^0 with long lifetimes using a $K^+ \to \pi^+\nu\bar{\nu}$ type of analysis has already been reported in Ref. 9.

A limit can also be placed on a light Higgs boson (H^0) in the minimal standard model in the mass region of $m_{H^0} < 100$ MeV/c^2. Other experiments covering similar Higgs-boson mass regions have been reported.[13] Assuming the mass dependence of the Higgs-boson lifetime given in Ref. 14, the upper limit for the combined branching ratio $B(K^+ \to \pi^+H^0, H^0 \to \gamma\gamma)$ is shown as a dashed line in Fig. 3.

For the π^+ spectrum from direct $K^+ \to \pi^+\gamma\gamma$ decay calculated with a phase-space distribution (assuming a unit matrix element as in Ref. 7), Table I shows that the net acceptance is 5.2×10^{-4}. Since no events were observed in the signal region, we set a 90%-confidence-level

upper limit for the branching ratio, $B(K^+ \to \pi^+ \gamma\gamma) < 1.0 \times 10^{-6}$. However, the spectrum is strongly model dependent and could be quite different from the phase-space distribution. For instance, by taking the ChPT distribution assumed in Ref. 5, the net acceptance would be 3.4×10^{-6}, resulting in a branching-ratio upper limit of 1.5×10^{-4}. This limit is still 3 orders of magnitude higher than the ChPT prediction. For the phenomenological model incorporating broken SU(3) symmetry[3] whose predictions for $K^+ \to \pi^+ \gamma\gamma$ were not ruled out by previous experiments, our result sets an upper limit of 2.3×10^{-6} which is not consistent with the predicted range of branching ratios of $(6\text{–}20) \times 10^{-6}$. Other models such as the axial-vector-dominance model[1] and the pole modes with virtual π^0 or η intermediate states[2] have been ruled out by earlier experiments and are similarly inconsistent with the present results.

This research was supported in part by the U.S. Department of Energy under Contracts No. DEAC02-76CH00016, No. W-7405-ENG-36, and No. DE-AC02-76ER03072, and by the Natural Sciences and Engineering Research Council and the National Research Council of Canada.

---

[a]Present address: Princeton University, Princeton, NJ 08544.

[b]Present address: Cornell University, Ithaca, NY 14853.

[c]Present address: Université de Montréal, Québec, Canada H3C 3J7.

[1]G. W. Intemann, Phys. Rev. D **2**, 2630 (1970).

[2]Y. Fujii, Phys. Rev. Lett. **17**, 22 (1966); I. R. Lapidus, Nuovo Cimento **46**, 668 (1966); L. M. Brown *et al.*, Phys. Rev. D **4**, 146 (1971).

[3]M. Moshe and P. Singer, Phys. Rev. D **6**, 1379 (1972).

[4]G. Ecker, A. Pich, and E. de Rafael, Nucl. Phys. **B303**, 665 (1988); **B291**, 692 (1987); Phys. Lett. B **189**, 363 (1987); J. Gasser and H. Leutwyler, Ann. Phys. (N.Y.) **158**, 142 (1984).

[5]H-Y. Cheng, Phys. Rev. D **42**, 72 (1990).

[6]G. Ecker, A. Pich, and E. de Rafael, Phys. Lett. B **237**, 481 (1990).

[7]Y. Asano *et al.*, Phys. Lett. **113B**, 195 (1982).

[8]For axions, R. D. Peccei and H. R. Quinn, Phys. Rev. Lett. **38**, 1440 (1977); S. Weinberg, Phys. Rev. Lett. **40**, 223 (1978); F. Wilczek, Phys. Rev. Lett. **40**, 279 (1978); M. Dine, W. Fischler, and M. Srednicki, Phys. Lett. **104B**, 199 (1981). For *familons*, F. Wilczek, Phys. Rev. Lett. **49**, 1549 (1982). For *majorons*, Y. Chikashige, R. N. Mohapatra, and R. D. Peccei, Phys. Rev. Lett. **45**, 1926 (1980); Phys. Lett. **98B**, 265 (1981); G. B. Gelmini and M. Roncadelli, Phys. Lett. **99B**, 411 (1981); C. S. Aulakh and R. N. Mohapatra, Phys. Lett. **119B**, 136 (1982); S. Bertolini and A. Santamaria, Nucl. Phys. **B315**, 558 (1989).

[9]M. S. Atiya *et al.*, Phys. Rev. Lett. **64**, 21 (1990).

[10]J. S. Frank and R. C. Strand, in *Proceedings of the Workshop on Scintillating Fiber Detector Development for the Superconducting Super Collider,* edited by D. Anderson *et al.* (Fermi National Accelerator Laboratory, Batavia, IL, 1988).

[11]J. V. Cresswell *et al.*, IEEE Trans. Nucl. Sci. **35**, 460 (1988).

[12]M. S. Atiya *et al.*, Nucl. Instrum. Methods Phys. Res., Sect. A **279**, 180 (1989).

[13]D. Decamp *et al.*, Phys. Lett. B **236**, 233 (1990); G. D. Barr *et al.*, Phys. Lett. B **235**, 356 (1990); S. Egli *et al.*, Phys. Lett. B **222**, 533 (1989); P. Yepes, CERN Report No. CERN-EP/90-02 (to be published).

[14]J. Ellis, M. K. Gaillard, and D. V. Nanopoulos, Nucl. Phys. **B106**, 292 (1976); A. I. Vainshtein, V. I. Zakharov, and M. A. Shifman, Usp. Fiz. Nauk **131**, 537 (1980) [Sov. Phys. Usp. **23**, 429 (1980)]; S. Raby, G. B. West, and C. M. Hoffman, Phys. Rev. D **39**, 828 (1989).

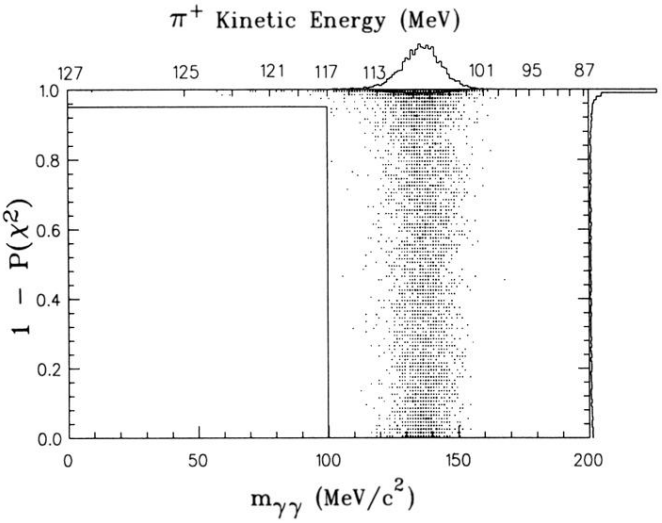

FIG. 2. Scatter plot of $m_{\gamma\gamma}$ vs $1-P(\chi^2)$ for the final sample of $K^+ \to \pi^+\gamma\gamma$ type of events.